Electronic Supplementary Material (ESI) for ChemComm.


# SUPPORTING INFORMATION

**Fibrinogen aptamer functionalized gold-coated iron-oxide nanoparticles for targeted imaging of thrombi**

Anna Koudrina, [a] Celine Chartrand, [a] Greg O Cron, [b,c,d] Jonathan O'Brien, [d] Eve C Tsai, [b,c,d] and Maria C DeRosa [a]*

a. Department of Chemistry, Carleton University, 1125 Colonel By Dr, Ottawa, ON K1S 5B6.

b. Ottawa Hospital Research Institute, 1053 Carling Ave, Ottawa, ON K1Y 4E9.

c. University of Ottawa, 75 Laurier Ave. E, Ottawa, ON K1N 6N5.

d. The Ottawa Hospital, 501 Smyth Rd, Ottawa, ON K1H 8L6

* E-mail: maria.derosa@carleton.ca

## Materials and methods

### 1.1 Chemicals and instruments

Iron (III) acetylacetonate ($Fe(acac)_3$), 99%, phenyl ether (99%), oleic acid (99%), oleylamine (70%), anhydrous sodium citrate (99%), 4-dimethyl(amino)pyridine (99%), hexanes, and absolute ethanol were purchased from SigmaAldrich (Oakville, ON, Canada). 1,2-hexadecanediol was purchased from TCI (Portland, Oregon, USA). Gold (III) acetate ($Au(ac)_3$) was purchased from Alpha Aesar (Haverhill, Massachusetts, USA). 300 mesh x 83 μm pitch copper Transmission Electron Microscopy (TEM) grids were purchased from Electron Microscopy Sciences (Hatfield, Pennsylvania, USA). All glassware used for the $Fe_3O_4$-AuNP synthesis was washed with aqua regia (3:1 mixture concentrated $HCl/HNO_3$) and rinsed thoroughly with deionized water. The glassware was then rinsed with acetone before being dried in an overnight or until used for synthesis. Unless otherwise stated, all synthetic procedures were performed using standard Schlenk techniques under an argon (5.0, 99.999 %) atmosphere.

All DNA was synthesized using Bioautomation MerMade 6 oligonucleotide synthesizer (Plano, TX, USA), using standard phosphoramidite chemistry. Phosphoramidites, synthesis reagents, and thiol C6 S-S modifier were all purchased from Glen Research (Sterling, VA, USA). Ultra-High Purity 5.0 argon was purchased from Praxair Canada (Mississauga, ON, Canada). Standard support columns and acetonitrile were purchased from BioAutomation (Plano, TX, USA). All DNA was purified using Glen-Pak cartridges purchased from Glen Research (Sterling, VA, USA) using the appropriate protocol for the modifier used during the synthesis. All purified DNA was sent to Novatia, LLC (Monmouth Jct, NJ, USA) in order to obtain molecular weight confirmation of the products by ESI-MS. De-salting and separation after the cleavage of the disulfide bond was done using Amicon-Ultra 0.5 mL 3 kDa cut-off ultra-centrifugal units purchased from Fisher Scientific Canada (Ottawa, ON, Canada).

Blood was obtained from The Ottawa Hospital Research Institute with approval from the Ottawa Health Science Network Research Ethics Board, OHSN-REB (application # 20150544-01H). All MR Imaging was done using an animal GE/Agilent MR901 Discovery 7T MRI Scanner (The University of Ottawa, Preclinical Imaging Core). All CT Imaging was done using General Electric HD 750 Discovery CT Scanner (The University of Ottawa).

## 1.2 Preparation of iron oxide ($Fe_3O_4$) nanoparticles

$Fe_3O_4$ nanoparticle seeds (as well as the final $Fe_3O_4$-AuNPs) were synthesized using a previously established protocol by Smith *et al.*[1] In brief, 0.71 g $Fe(acac)_3$ (2 mmol) was mixed in 20 mL of phenyl ether with 2 mL of oleic acid (~6 mmol) and 2 mL of oleylamine (~4 mmol) under argon atmosphere with vigorous stirring. Once dissolved, 2.58 g of 1,2-hexadecanediol (10 mmol) was added into the solution and a water-cooled condenser was affixed to the flask. The final solution was slowly heated to 210 °C (without exceeding this temperature) and refluxed for 2 h. After 2 h, a colour change was observed with bright red suspension turning dark brown. The reaction solution was cooled to room temperature under argon overnight and used directly in the subsequent step without separation.

## 1.3 Direct coating of $Fe_3O_4$ nanoparticles to produce $Fe_3O_4$-AuNPs

10 mL of the phenyl ether reaction solution of $Fe_3O_4$ nanoparticles (~0.33 mmol $Fe_3O_4$) were added to 30 mL of phenyl ether with vigorous stirring. To that, 0.83 g of $Au(ac)_3$ (2.2 mmol), 3.1 g of 1,2-hexadecanediol (12 mmol), 0.5 mL of oleic acid (~1.5 mmol), and 3 mL of oleylamine (~6 mmol) were added quickly. The mole ratio of the Au precursor to the iron oxide nanoparticles was approximately 7:1. Under argon atmosphere and with vigorous stirring, the reaction solution was heated slowly to 180-190 °C (10 °C/min) and was maintained at this temperature under reflux for 3 h. The reaction solution was cooled to room temperature under argon overnight. 5 mL of the cooled solution was combined with 15 mL of ethanol and agitated gently, resulting in visible aggregation of nanoparticles. The aggregates were magnetically separated by placing the flask on top of 6 rare earth magnets for 5-10 mins. The resulting supernatant was decanted as waste and the precipitated nanoparticles were washed three times with 15 mL of absolute ethanol. The nanoparticles were redispersed in 10 mL of hexanes, containing equal parts oleic acid and oleylamine (~75 mM, 0.25 mL). This procedure was repeated several times in order to obtain the necessary volume of $Fe_3O_4$-AuNPs.

## 1.4 Sodium citrate ligand exchange and conjugation with aptamer

The following steps were not performed under argon atmosphere. 5 mL of previously prepared $Fe_3O_4$-AuNPs in hexanes was precipitated as above, by magnetic separation using 15 mL of ethanol. The nanoparticles were washed three times with 15 mL of absolute ethanol and redispersed in 3 mL of 1M TMAOH containing 0.2 g of sodium citrate. The pH of solution was slowly adjusted to approximately 6.5 with dilute HCl. The solution was sonicated at room temperature for 15 mins. The nanoparticles were

subsequently collected using a magnet and redispersed in 5 mL of Milli-Q deionized water and sonicated for a further 5 mins at room temperature.

Thiol-FA/FB139 (60 nmol) was vortexed in 75 µL of 50 mM Tris (pH 8.4) containing 100 mM dithiothreitol (DTT) at ambient temperature for 30 minutes in order to cleave the 5'-disulfide in preparation for conjugation with $Fe_3O_4$-AuNPs. Cleaved FA/FB139 was washed using BioRad Micro Bio-Spin Chromatography columns with EDTA buffer (7 mM, pH 7.0) and subsequently de-salted using Amicon Ultra 0.5 mL Centrifugal Filters with HEPES buffer (50 mM, 7 mM EDTA, pH 7.0). An aliquot of the final solution of $Fe_3O_4$-AuNPs (100 µL) was then combined with 100 µL of thiolated (cleaved, 100 µM) FA/FB139. This was shaken overnight to allow for surface-functionalization. In order to remove any unbound sequences, FA/FB139-$Fe_3O_4$-AuNPs were collected on a rare earth magnet, decanting the remaining solution. They were subsequently redispersed in deionized water and sonicated for 5 mins at room temperature.

### 1.5 Characterization of $Fe_3O_4$-AuNPs

UV-Vis absorption characterization of the $Fe_3O_4$-AuNPs was performed using a Cary 300 Bio UV-Visible spectrophotometer (Varian, Santa Clara CA). Peaks at 404 nm and 530-540 nm corresponded to the $Fe_3O_4$-core and thin Au-coating, respectively, and concentrations were calculated using $3 \times 10^8$ $M^{-1}$ $cm^{-1}$ as the gold coating molar extinction coefficient. In order to ensure the appropriate amount of contrast material ($Fe_3O_4$) is present, all subsequent treatment concentrations were calculated based on the Au-coating, assuming that any of the non-coated material had been separated away in previous steps. $Fe_3O_4$-AuNPs were analyzed at every step of the synthesis using TEM images taken with a FEI Technai G2 F20 TEM at the Carleton University Nano-imaging Facility, with a field emission source at a voltage of 200 kV using Gatan Microscopy Suite 2V. All images were taken on dry 300 mesh x 83 µm pitch carbon coated copper TEM grids at room temperature. Grids were prepared by placing 4 µL of $Fe_3O_4$-AuNP (in various solvents) directly on top, followed by minimum 4 h of drying. Likewise, at each step of the synthesis, $Fe_3O_4$-AuNPs were analyzed with (EDS) at a 20° take off angle with an Oxford X-max 80 mm EDS detector using Aztec software. TEM images were analyzed for nanoparticle size distribution using ImageJ Software by changing the scale of the image from metres to pixels.

### 1.6 Assessment of magnetic properties of FA-$Fe_3O_4$-AuNPs

To evaluate if surface functionalization of $Fe_3O_4$-AuNPs with FA and the subsequent binding of FA-$Fe_3O_4$-AuNPs to fibrin perturbs the magnetic properties, 100 µL of 60 nM FA-$Fe_3O_4$-AuNPs was incubated

with 0.005 g of lyophilized fibrin from human plasma for 1 hour. As a control, fibrin was incubated with bare $Fe_3O_4$-AuNPs. After incubation, all samples were washed 10x with PBS buffer (pH 7.4) to wash away unbound nanoparticles. Rare earth magnet was used to assess whether FA-$Fe_3O_4$-AuNPs-bound fibrin would exhibit magnetic properties.

## 1.7 T2-weighted MRI

***Transverse relaxivity measurements.*** FA-$Fe_3O_4$-AuNPs were prepared in PBS (pH 7.4) to concentrations of 0.006, 0.015, 0.030, 0.045, and 0.060 µM. The pulse sequence for the T2 map followed the spin echo technique, with eight time points at 11.8, 17.6, 23.5, 29.4, 35.3, 41.2, 47.0, and 52.9 ms; repetition time 6000 ms; matrix size 256 × 256. Volume resonator body 150 mm coil was used for all relaxivity measurements. The signal intensities were measured using a predetermined round region of interest (ROI) with ImageJ software. Relaxation rate ($1/T_n$, n = 2) was plotted against concentration, and the slope of the linear fit was used to deduce transverse relaxivity.

***In vitro samples.*** Whole human blood was clotted using a previously established thrombectomy protocol.[2] In brief, 1 mL of $CaCl_2$-thrombin solution was prepared using 0.252M $CaCl_2$ and 100 U of thrombin. This solution was subsequently mixed with 5 mL of whole blood and left to form a clot at room temperature for 30 minutes. The large clots were sectioned into smaller clots, approximately 1 cm by 1 cm in size. Each blood clot was combined with 1 mL of either heparinized blood or PBS buffer (pH 7.4). To each sample, 100 µL of 60 nM FA-$Fe_3O_4$-AuNPs (or FB139-$Fe_3O_4$-AuNPs for control treatments) was injected and left to incubate for 45 mins to allow for equilibration of the interaction of the aptamer with the fibrin target. T2-weighted scans (7 Tesla, echo time=42 ms, repetition time ≥ 6000 ms) were performed over a 20-minute span. Volume resonator body 150 mm coil was used for all imaging. Signal intensities of the T2-weighted scans were measured using a circular ROI with ImageJ software. Enhancement achieved in incubations of FA-$Fe_3O_4$-AuNPs with blood clots suspended in blood pool or PBS was compared to the control treatments of blood clots with FB139-$Fe_3O_4$-AuNPs and PBS. FB139 was chosen as the control sequence, as it is similar in length and characteristics, but was originally selected for a different target (toxin).[3]

## 1.8 CT imaging

***Contrast (HU) measurements.*** FA-$Fe_3O_4$-AuNPs were prepared in PBS (pH 7.4) to concentrations of 0.006, 0.015, 0.030, 0.045, and 0.060 µM, while Isovue (clinically available CT contrast material) was diluted to concentrations of 0.1, 0.25, 0.50, 0.75, and 1 mM. Imaging was conducted using dual energy protocols at 80−140 kVp. Contrast (HU) was measured using The Ottawa Hospital PACS software.

***In vitro samples.*** Blood clots were produced from human blood using the same protocol as in section 1.7. Each blood clot was combined with 1 mL of either heparinized blood or PBS buffer (pH 7.4) and samples were set up in triplicate. To each sample, 100 µL of 60 nM FA-$Fe_3O_4$-AuNPs (or FB139-$Fe_3O_4$-AuNPs for control treatments) was injected and left to incubate for 45 mins. All CT Imaging was done using dual energy protocols at 80-140 kVp. Contrast enhancement (HU) was analyzed with The Ottawa Hospital PACS software.

## Additional results and discussion

Unfortunately, as it relates to $Fe_3O_4$-AuNPs, a number of synthesis-related constraints have been identified. Among other parameters, it is important but challenging to control for the overall size and monodispersity.[4,5] Since $Fe_3O_4$ NPs tend to be relatively unstable, which leads to aggregation, several methods of functionalization to increase biocompatibility have been proposed. Nevertheless, this is difficult to implement, as $Fe_3O_4$ NPs are not compatible with many surface chemistry modifications, and furthermore, it is tricky to control the uniformity of the coating.[6,7] Using the previously optimized method by Smith *et al*., $Fe_3O_4$-core was synthesized and coated with a thin layer of Au to allow for subsequent direct incorporation of FA. Disulfide-modified FA was first reacted with dithiothreitol in order to cleave the disulfide bond and liberate a free reactive thiol group. It was then combined with the final $Fe_3O_4$-AuNPs to achieve FA-functionalized CSN (Sch S1).[1,8] Since a number of washes were required at each step of the synthesis and involved collection of the nanoparticles on rare earth magnets, it was confirmed that neither the gold-coating, nor the aptamer-conjugation perturbed the magnetic properties. It has previously been reported that saturation magnetization ($M_S$) of non-bulk phase iron oxide nanoparticles possess an experimental value in the range of 30-80 emu $g^{-1}$. The thin gold coating results in a slight drop of $M_S$ to approximately 16-30 emu $g^{-1}$, indicating that the effect on the inner $Fe_3O_4$ NP is minimal.[9,10] Furthermore, surface functionalization does not significantly impact saturation magnetization, which crucial for providing contrast enhancement in T2-weighted MRI (magnetic properties confirmed in Fig S5).[7] The structure and morphology of each synthesized component was confirmed by transmission electron microscopy (TEM) and energy-dispersive X-ray spectroscopy (EDS) (Fig S1-S3). Size distribution was measured using ImageJ software and the final formulation was determined to be 5.42±0.72 nm in diameter (Fig S3). Synthesized $Fe_3O_4$-AuNPs and FA-$Fe_3O_4$-AuNPs were quantified by UV-Vis absorption spectroscopy, monitoring for peaks in the 535-550 nm range, corresponding to the gold coating, and 260 nm, corresponding to DNA (Fig S4).[11] Maximum absorption for FA-$Fe_3O_4$-AuNPs underwent a red-shift, which was attributed to surface functionalization and is commonly observed.[10] The final concentration was calculated to be 60 nM based on an extinction coefficient of $3 \times 10^8$ $M^{-1}$ $cm^{-1}$ for the gold-coating and estimated aptamer coverage varied from 130 to 215 aptamers per nanoparticle as judged by UV-Vis spectroscopy.

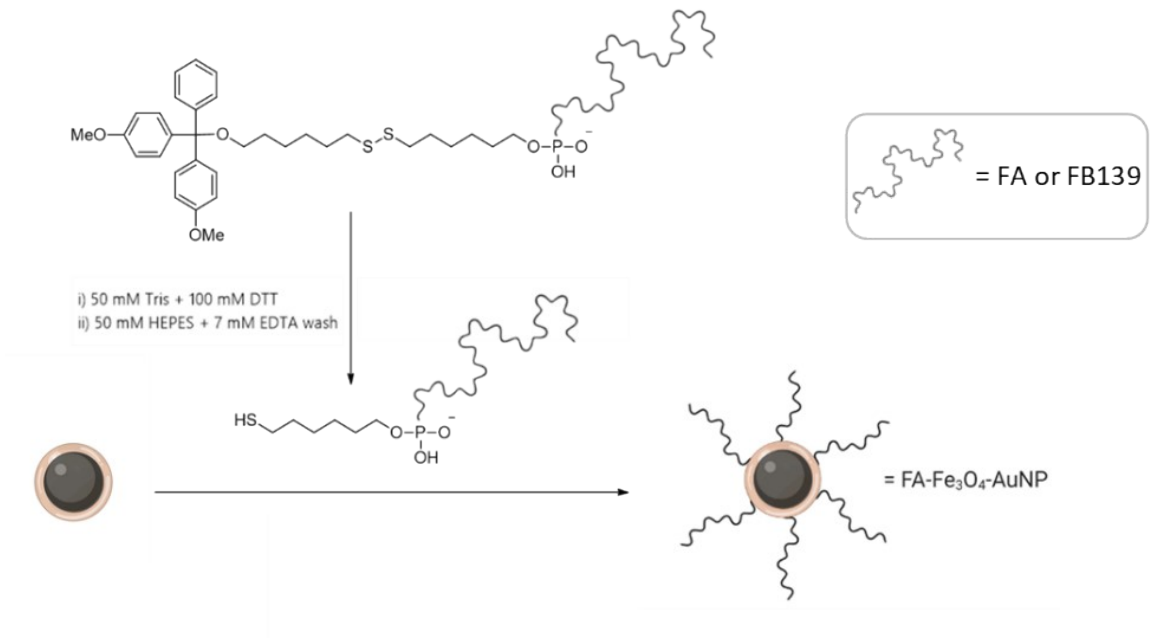


**Scheme S1: Reaction scheme outlining the synthesis of FA-$Fe_3O_4$-AuNPs. FA was synthesized with a 5' DMT-protected thiol C6 S-S modifier, the disulfide bond of which was cleaved with DTT at ambient temperature for 30 minutes to liberate a free thiol group; subsequently, the free thiol group was used to create the Au-S bond in order to conjugate FA to the surface of $Fe_3O_4$-AuNPs.**

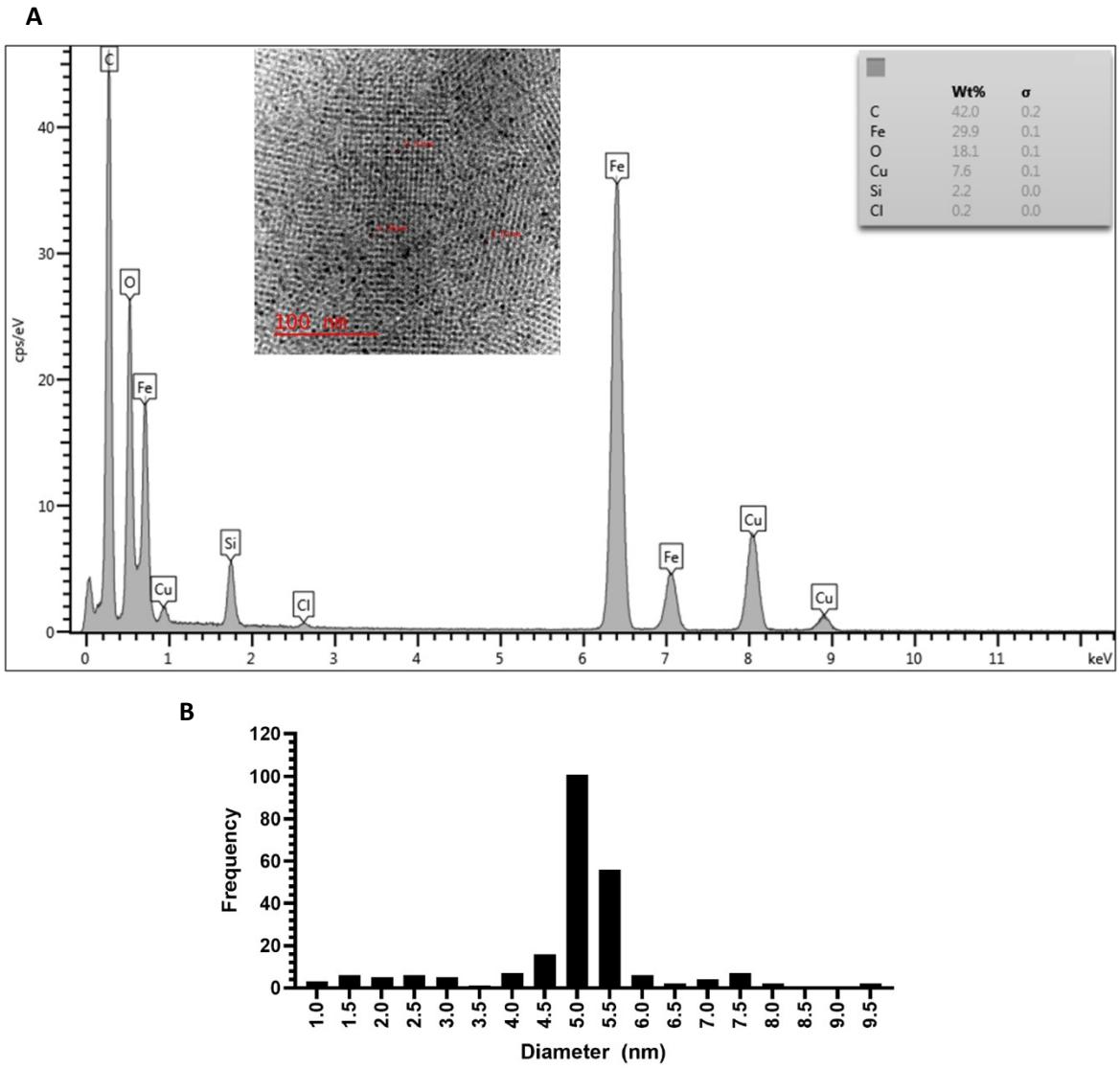


**Figure S1**: **(A) TEM image with 100 nm scale bar and corresponding energy-dispersive X-ray spectroscopy (EDS) spectrum of small, monodispersed $Fe_3O_4$-core. Strong EDS peaks for both Fe and O indicate the presence of iron oxide. (B) Histogram demonstrating the size distribution, with average diameter of 4.95±1.27 nm (n=229). Measured with ImageJ.**

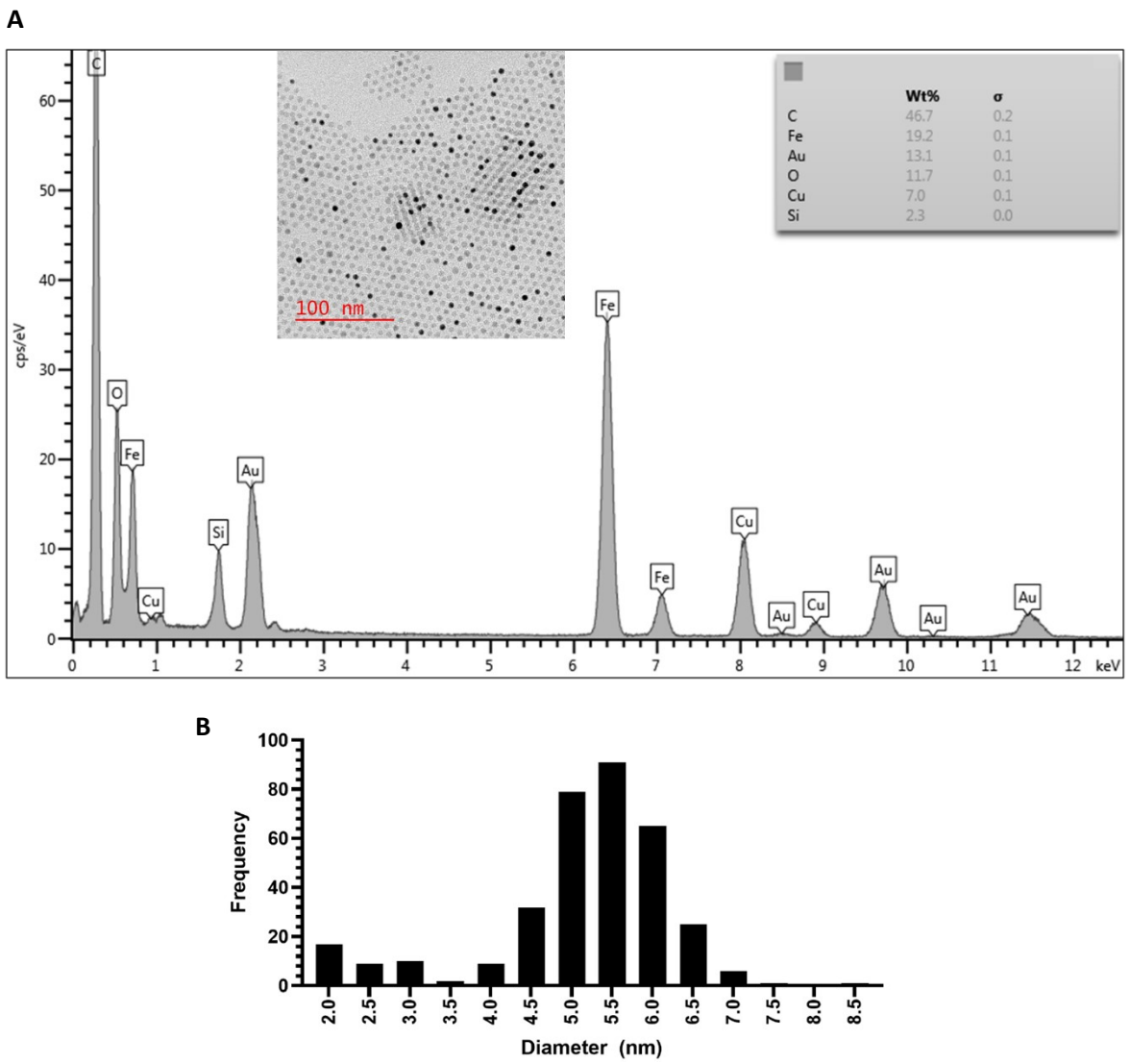


**Figure S2: (A) TEM image with 100 nm scale bar and corresponding EDS spectrum of the $Fe_3O_4$-AuNPs in phenyl ether. Strong EDS peaks for both Fe and O indicate the presence of iron oxide, while the presence of a peak for Au confirms gold-coating. (B) Histogram demonstrating the size distribution, with average diameter of 5.13±1.14 nm (n=347). Measured with ImageJ.**

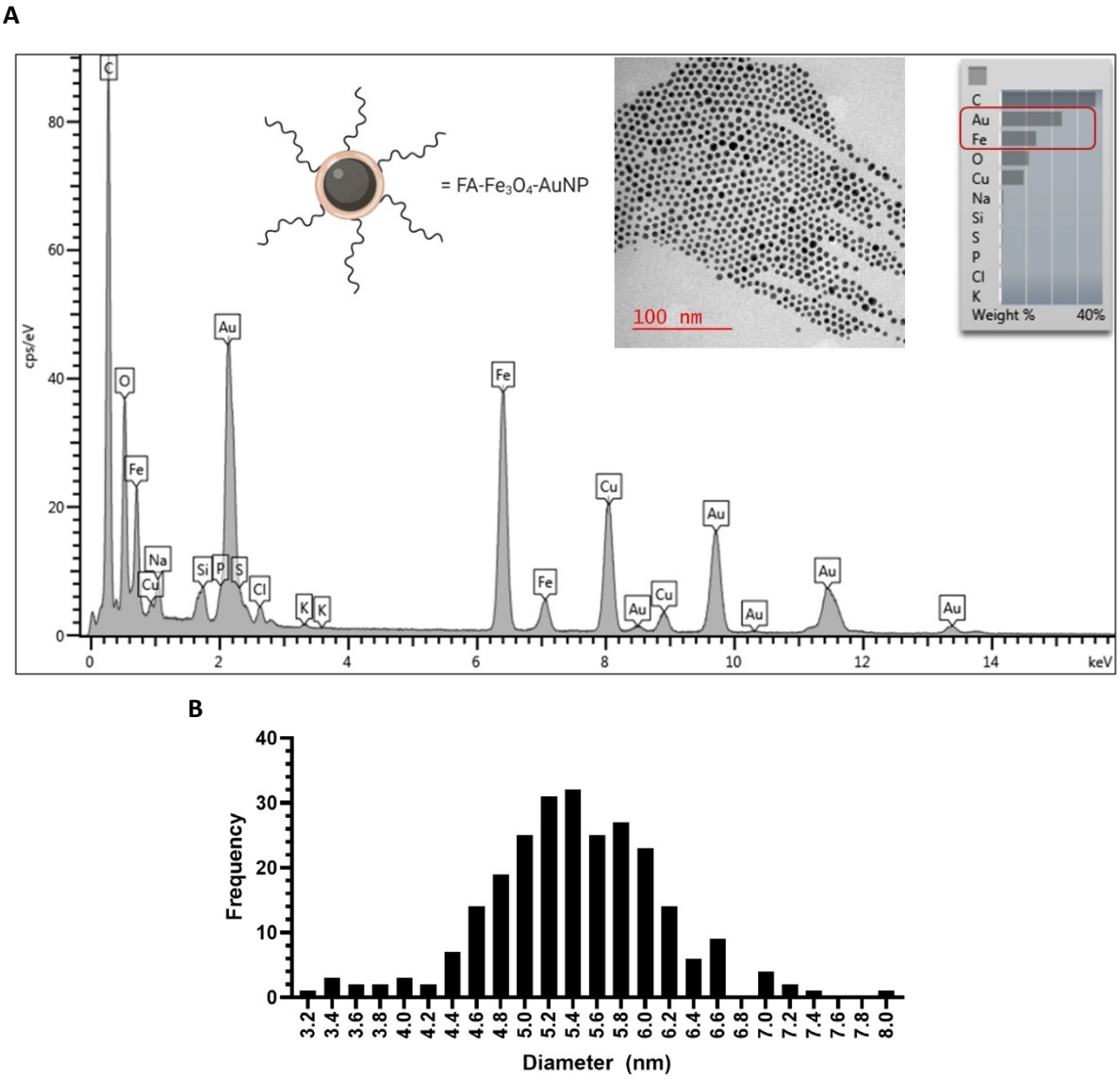


**Figure S3: TEM image with 100 nm scale bar and corresponding EDS spectrum of FA-$Fe_3O_4$-AuNPs in di$H_2O$. All nanoparticle components are preserved. (B) Histogram demonstrating the size distribution, with average diameter of 5.42±0.72 nm (n=253). Measured with ImageJ.**

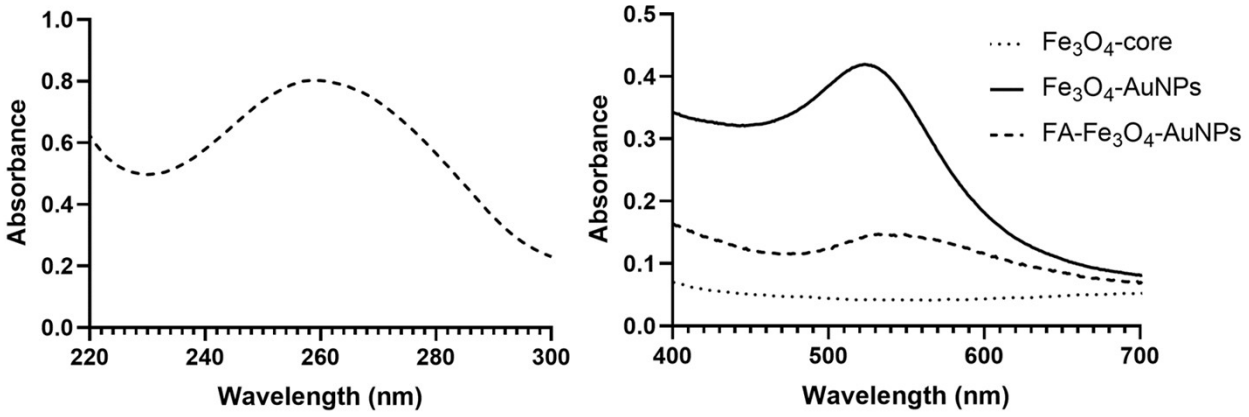


**Figure S4: UV-Vis spectra of $Fe_3O_4$-core, $Fe_3O_4$-AuNPs, and FA-$Fe_3O_4$-AuNPs in their respective buffers**

The ability of FA to bind fibrin has previously been confirmed.[12] In this formulation, it was important that such binding did not lead to loss of magnetic properties, as they are crucial to MRI. Incubation with FA-$Fe_3O_4$-AuNPs allowed for binding to occur, as evident by the presence of dark colour, associated with FA-$Fe_3O_4$-AuNPs bound on the surface of fibrin (Figure S5 – middle). This was not observed when fibrin was treated with bare $Fe_3O_4$-AuNPs, which also confirmed that PBS washes likely got rid of the majority of non-targeted nanoparticles (Figure S5 – left). Placing FA-$Fe_3O_4$-AuNPs treated fibrin on a magnet resulted in accumulation of the smaller sized particles in the middle, indicating that FA-$Fe_3O_4$-AuNPs retains its magnetic properties when bound to the target (Figure S5 – right).

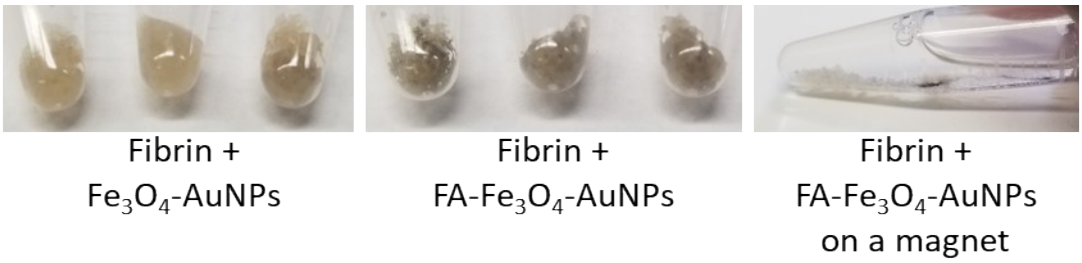


**Figure S5: Fibrin incubated with bare $Fe_3O_4$-AuNPs (left), FA-$Fe_3O_4$-AuNPs (middle), and magnetized fibrin (with bound FA-$Fe_3O_4$-AuNPs after 10x wash with PBS) on a rare earth magnet. Fibrin magnetization is demonstrated by accumulation of small dark powder concentrated to the middle.**

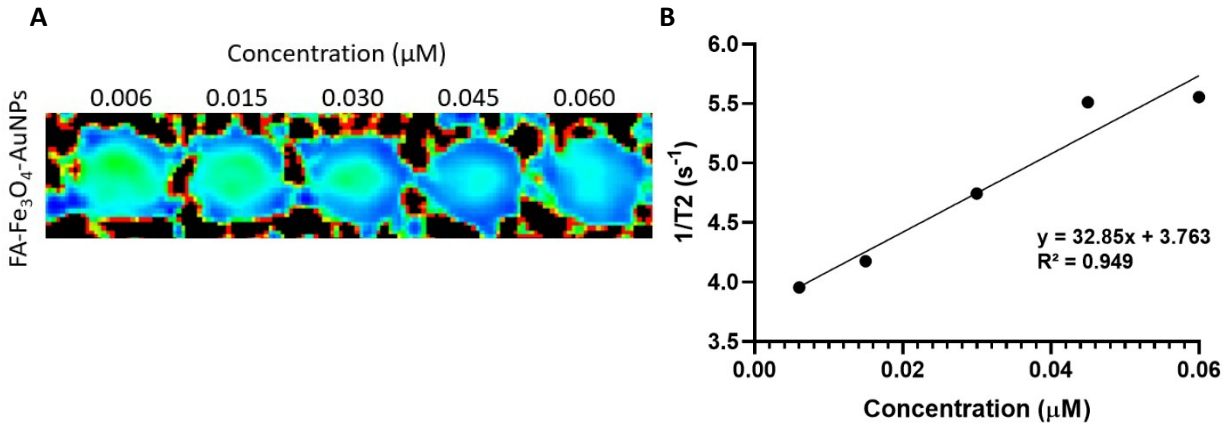


**Figure S6: (A) T2 map MR images over an increasing range of concentrations of FA-$Fe_3O_4$-AuNPs; (B) Transverse relaxivity plot of FA-$Fe_3O_4$-AuNPs, with a calculated r2 value of 32.85 $\mu M^{-1}s^{-1}$, obtained by the slope of the relationship between relaxation rates (1/T2) and contrast formulation concentration for each dilution.**

AuNPs have been researched for applications in CT imaging, due to many favourable characteristics of gold, including its ability exhibit higher X-ray attenuation than iodine.[13] With that in mind, increasing concentrations of FA-$Fe_3O_4$-AuNPs were tested for their capability to produce measurable CT contrast in the absence of a target. Concentrations achievable during the synthesis were considerably lower than that of Isovue, which was used as a control. Nevertheless, increasingly brighter contrast, represented in a shift from blue to red colour (Figure S7A), was observed for FA-$Fe_3O_4$-AuNPs at low micromolar concentrations, while Isovue failed to achieve any contrast above the baseline of water. The slope of the linear relationship between the measured contrast (HU) and the concentration was measured to be 1697 HU $\mu M^{-1}$ (Figure S7). Unfortunately, the susceptibility of FA-$Fe_3O_4$-AuNPs to dilution in the final volume of the samples was considerable, resulting in no observable contrast for any of the treatments with $Fe_3O_4$-AuNPs (Figure S8).

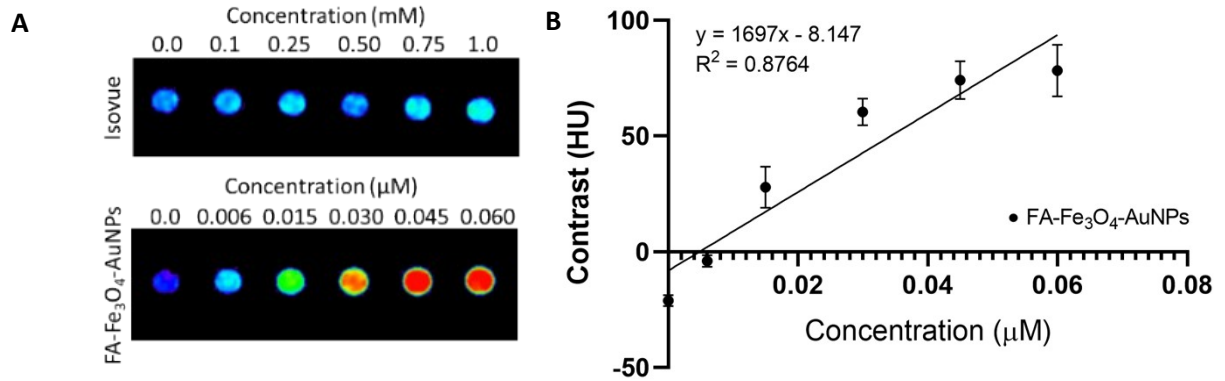

**Figure S7: (A) CT contrast phantom images of Isovue (iopamidol) and FA-FA-Fe3O4-AuNPs, both with increasing concentrations, at 100 kVp; (B) Plot of concentration-dependent contrast enhancement (HU), measured with software provided with the CT scanner, for FA-$Fe_3O_4$-AuNPs.**

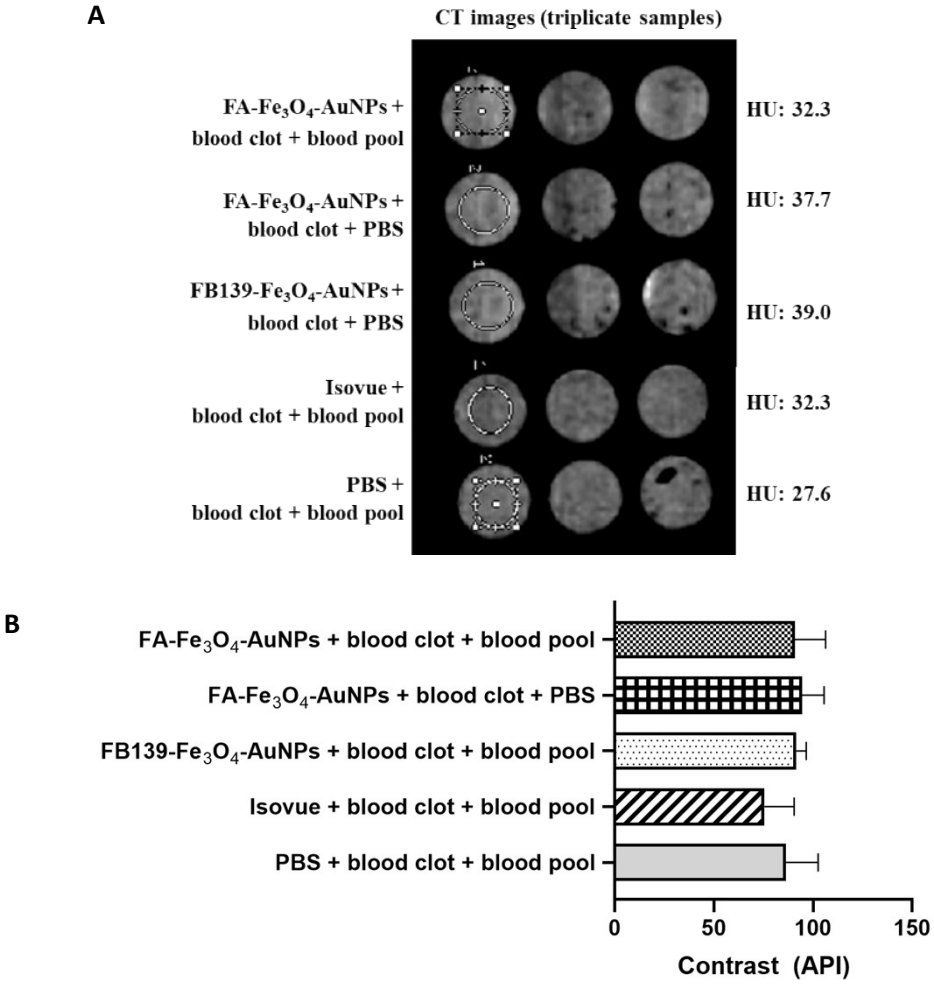


**Figure S8: (A) CT images of human blood clots 45-minutes after treatment with FA-$Fe_3O_4$-AuNPs, FB139-$Fe_3O_4$-AuNPs, Isovue, or PBS (pH 7.4), all treatments were done in triplicate; (B) Contrast, measured based on signal intensity using ImageJ software, associated with each treatment.**

**References**


(1) Smith, M.; McKeague, M.; DeRosa, M. C. Synthesis, Transfer, and Characterization of Core-Shell Gold-Coated Magnetic Nanoparticles. *MethodsX* **2019**, *6*, 333–354. https://doi.org/10.1016/j.mex.2019.02.006.

(2) Srinivasan, V. M.; Chen, S. R.; Camstra, K. M.; Chintalapani, G.; Kan, P. Development of a Recalcitrant, Large Clot Burden, Bifurcation Occlusion Model for Mechanical Thrombectomy. *Neurosurg. Focus* **2017**, *42* (4), 1–6. https://doi.org/10.3171/2017.1.FOCUS16501.

(3) McKeague, M.; Bradley, C. R.; de Girolamo, A.; Visconti, A.; David Miller, J.; DeRosa, M. C. Screening and Initial Binding Assessment of Fumonisin B1aptamers. *Int. J. Mol. Sci.* **2010**, *11* (12), 4864–4881. https://doi.org/10.3390/ijms11124864.

(4) Guardia, P.; Labarta, A.; Batlle, X. Tuning the Size, the Shape, and the Magnetic Properties of Iron Oxide Nanoparticles. *J. Phys. Chem. C* **2011**, *115* (2), 390–396. https://doi.org/10.1021/jp1084982.

(5) Blasiak, B.; Van Veggel, F. C. J. M.; Tomanek, B. Applications of Nanoparticles for MRI Cancer Diagnosis and Therapy. *J. Nanomater.* **2013**, *2013*, 1–12. https://doi.org/10.1155/2013/148578.

(6) Zamay, G. S.; Zamay, T. N.; Lukyanenko, K. A.; Kichkailo, A. S. Aptamers Increase Biocompatibility and Reduce the Toxicity of Magnetic Nanoparticles Used in Biomedicine. *Biomedicines* **2020**, *8* (59), 1–14.

(7) Moraes Silva, S.; Tavallaie, R.; Sandiford, L.; Tilley, R. D.; Gooding, J. J. Gold Coated Magnetic Nanoparticles: From Preparation to Surface Modification for Analytical and Biomedical Applications. *Chem. Commun.* **2016**, *52* (48), 7528–7540. https://doi.org/10.1039/c6cc03225g.

(8) Robinson, I.; Tung, L. D.; Maenosono, S.; Wälti, C.; Thanh, N. T. K. Synthesis of Core-Shell Gold Coated Magnetic Nanoparticles and Their Interaction with Thiolated DNA. *Nanoscale* **2010**, *2* (12), 2624–2630. https://doi.org/10.1039/c0nr00621a.

(9) Wu, W.; He, Q.; Jiang, C. Magnetic Iron Oxide Nanoparticles: Synthesis and Surface Functionalization Strategies. *Nanoscale Res. Lett.* **2008**, *3* (11), 397–415. https://doi.org/10.1007/s11671-008-9174-9.

(10) Zhou, H.; Lee, J.; Park, T. J.; Lee, S. J.; Park, J. Y.; Lee, J. Ultrasensitive DNA Monitoring by Au-Fe3O4 Nanocomplex. *Sensors Actuators, B Chem.* **2012**, *163* (1), 224–232. https://doi.org/10.1016/j.snb.2012.01.040.

(11) Wang, L.; Luo, J.; Fan, Q.; Suzuki, M.; Suzuki, I. S.; Engelhard, M. H.; Lin, Y.; Kim, N.; Wang, J. Q.; Zhong, C. J. Monodispersed Core-Shell Fe3O4@Au Nanoparticles. *J. Phys. Chem. B* **2005**, *109* (46), 21593–21601. https://doi.org/10.1021/jp0543429.

(12) Koudrina, A.; McConnell, E. M.; Zurakowski, J. A.; Cron, G. O.; Chen, S.; Tsai, E. C.; DeRosa, M. C. Exploring

Unique Contrast Properties of Aptamer-Gadolinium Conjugates in Magnetic Resonance Imaging for Targeted Imaging of Thrombi. *ACS Appl. Mater. Interfaces* **2020**, Manuscript ID: am-2020-166668.

(13) Mahan, M. M.; Doiron, A. L. Gold Nanoparticles as X-Ray, CT, and Multimodal Imaging Contrast Agents: Formulation, Targeting, and Methodology. *J. Nanom* **2018**, *2018*, 1–15.